MLL1 is essential for the senescence-associated secretory phenotype

Brian C. Capell,[1,2] Adam M. Drake,[1] Jiajun Zhu,[1] Parisha P. Shah,[1] Zhixun Dou,[1] Jean Dorsey,[1] Daniel F. Simola,[1] Greg Donahue,[1] Morgan Sammons,[1] Taranjit Singh Rai,[3,4] Christopher Natale,[2] Todd W. Ridky,[2] Peter D. Adams,[3] and Shelley L. Berger[1]

[1]Epigenetics Program, Department of Cell and Developmental Biology, University of Pennsylvania Perelman School of Medicine, Philadelphia, Pennsylvania 19104, USA; [2]Department of Dermatology, University of Pennsylvania Perelman School of Medicine, Philadelphia, Pennsylvania 19104, USA; [3]Institute of Cancer Sciences, Beatson Laboratories, University of Glasgow, Glasgow G611BD, United Kingdom; [4]Institute of Biomedical and Environmental Health Research, University of the West of Scotland, Paisley PA12BE, United Kingdom

Oncogene-induced senescence (OIS) and therapy-induced senescence (TIS), while tumor-suppressive, also promote procarcinogenic effects by activating the DNA damage response (DDR), which in turn induces inflammation. This inflammatory response prominently includes an array of cytokines known as the senescence-associated secretory phenotype (SASP). Previous observations link the transcription-associated methyltransferase and oncoprotein MLL1 to the DDR, leading us to investigate the role of MLL1 in SASP expression. Our findings reveal direct MLL1 epigenetic control over proproliferative cell cycle genes: MLL1 inhibition represses expression of proproliferative cell cycle regulators required for DNA replication and DDR activation, thus disabling SASP expression. Strikingly, however, these effects of MLL1 inhibition on SASP gene expression do not impair OIS and, furthermore, abolish the ability of the SASP to enhance cancer cell proliferation. More broadly, MLL1 inhibition also reduces "SASP-like" inflammatory gene expression from cancer cells in vitro and in vivo independently of senescence. Taken together, these data demonstrate that MLL1 inhibition may be a powerful and effective strategy for inducing cancerous growth arrest through the direct epigenetic regulation of proliferation-promoting genes and the avoidance of deleterious OIS- or TIS-related tumor secretomes, which can promote both drug resistance and tumor progression.

Numerous DNA-damaging cellular stresses, including both oncogene activation and DNA-damaging chemotherapeutics, may lead to cellular senescence (van Deursen 2014). Although senescent cells are tumor-suppressive, they paradoxically possess deleterious effects through the secretion of numerous inflammatory cytokines and growth factors known as the senescence-associated secretory phenotype (SASP) (Coppe et al. 2010). Indeed, the SASP is a driving force behind the low-level chronic inflammation that causes or exacerbates many age-related diseases, such as cancer (Rodier and Campisi 2011; Munoz-Espin and Serrano 2014). SASP secretion leads to pleiotropic effects, including the pathological increased proliferation of premalignant and malignant cells (Coppe et al. 2006; Wang et al. 2006; Neves et al. 2015). Hence, approaches to separate the beneficial tumor-suppressive growth arrest of senescence from the deleterious secretion of the SASP would be of significant clinical value (Coppe et al. 2010; Munoz-Espin and Serrano 2014; van Deursen 2014). Indeed, recent studies have shown that the mechanism of the anti-aging and anti-cancer effects of the diabetes medication metformin may be through SASP inhibition (Algire et al. 2012; Moiseeva et al. 2013).

Given these important roles and consequences, the SASP is regulated at multiple levels, involving various transcription factors (NF-κB and C/EBPβ) (Kuilman et al. 2008; Chien et al. 2011) and kinases (p38MAPK and protein kinase D1) (Freund et al. 2011; Wang et al. 2014). Importantly, however, activation of the DNA damage response (DDR) is fundamentally required for SASP activation (Di Micco et al. 2006; Rodier et al. 2009; Coppe et al. 2011). In contrast, mechanisms that underlie epigenomic regulation of the SASP are relatively unknown.

Corresponding author: bergers@mail.med.upenn.edu
Article is online at http://www.genesdev.org/cgi/doi/10.1101/gad.271882.115.

Therefore, given the critical role of the transcriptional activator and oncoprotein MLL1 in the mammalian DDR (Liu et al. 2010; Rao and Dou 2015), we investigated the role of MLL1 in SASP expression. We demonstrate that MLL1 is required for the expression of proproliferative cell cycle genes that are, in turn, necessary for triggering the DDR and its resulting inflammatory signaling pathways, including the SASP. Our results provide evidence that MLL1 inhibition may be an important therapeutic strategy to inhibit the potentially deleterious aspects of both the oncogene-induced senescence (OIS)-induced and therapy-induced senescence (TIS)-induced SASP and SASP-like inflammation while avoiding senescence escape and cancer. Indeed, as increasing evidence suggests that therapy-induced inflammation can lead to tumor progression, drug resistance, and metastasis (Obenauf et al. 2015; Shalapour and Karin 2015; Zelenay et al. 2015), MLL1 may prove an ideal primary or adjuvant target in order to simultaneously inhibit cancerous proliferation and the inflammatory side effects.

Results

MLL1 inhibition dramatically attenuates SASP expression

We used a standard model of DNA damage-induced OIS via 4-hydroxytamoxifen (4-OHT)-induced expression of the H-Ras V12 (Serrano et al. 1997) oncogene in IMR90 fibroblasts. Senescence was confirmed by standard senescence-associated β-galactosidase (SA-β-gal) staining (Supplemental Fig. S1A,B) and other markers of senescence using RNA sequencing (RNA-seq), such as up-regulation of the tumor suppressor *CDKN2A* and down-regulation of cyclin-dependent kinase genes such as *CDK2* and the nuclear lamina protein and senescence marker, *LMNB1* (Supplemental Fig. S1C). We examined the effect of MLL1 ablation on SASP expression in senescence using shRNAs designed against MLL1 mRNA. As a control, we treated both normal proliferating cells and OIS cells with scrambled control (SC) shRNAs (referred to as SC and SC OIS, respectively, hereafter). As expected, in OIS, MLL1 shRNA-treated cells (MLL1 knockdown CTL and MLL1 knockdown OIS, respectively) consistently displayed decreased levels of MLL1 in comparison with SC OIS cells (Supplemental Fig. S1D,E).

Using RNA-seq, we identified the most up-regulated genes (>1.5-fold increase in mRNA expression) from scrambled control (SC) cells to SC OIS as well as the most down-regulated genes (>1.5-fold decrease in mRNA expression) from SC OIS to MLL1 knockdown OIS (Supplemental Table 1). These criteria identified 224 genes, which represented the most differentially expressed in OIS with and without MLL1 ablation. Gene ontology (GO) analysis of these genes identified numerous categories associated with the SASP (i.e., "cytokine activity" contained the most genes, while others included "chemokine activity," "cytokine receptor binding," "growth factor activity," and "growth factor receptor binding"; fold enrichment > 5, $P < 0.05$) (Supplemental Fig. S1F).

Direct examination of the top 20 most highly up-regulated SASP genes identified in this analysis demonstrated broad and dramatic reductions in expression of canonical SASP genes (Freund et al. 2010) in MLL1 knockdown OIS cells compared with SC OIS cells ($P = 0.03$ for SASP gene reduction; $P = 0.18$ for all other genes) (Fig. 1A). For example, *IL1β*, a key inflammasome mediator and the most highly up-regulated of all genes in the RNA-seq data set, was reduced almost fivefold (Fig. 1A, far left). Other genes with profound reductions in expression included standard SASP genes such as *IL1A*, *IL8*, *IL6*, *MMP1*, and *MMP3* (Fig. 1A). We confirmed these results by RT-qPCR to examine expression of three representative SASP genes, *IL1A*, *IL1B*, and *IL8* (Fig. 1B), given that they are the most highly up-regulated SASP genes in IMR90 OIS (including in our RNA-seq data) (Freund et al. 2010) and because IL1α has a critical upstream role in inducing many downstream SASP factors (Acosta et al. 2013). Furthermore, these specific genes are emerging as critical potential targets in numerous human cancers (Crusz and Balkwill 2015). We further verified these results using a second MLL1 shRNA, which recapitulated the reduction in SASP gene expression via RT-qPCR (Supplemental Fig. S1G). As an additional confirmation of SASP reduction in MLL1 knockdown OIS cells, we performed enzyme-linked immunosorbent assays (ELISAs). This assay assesses secreted levels of canonical SASP factors within conditioned medium derived from either SC OIS or MLL1 knockdown OIS cells. The ELISAs showed a clear reduction of all tested SASP factors from MLL1 knockdown OIS cells compared with SC OIS (Fig. 1C) in multiple biological replicates. For example, SASP factors such as IL6, which has been implicated in cancer-associated inflammation (Crusz and Balkwill 2015), displayed a striking reduction of ~13-fold in MLL1 knockdown OIS conditioned medium (Fig. 1C). Similarly, we performed Western blotting for IL1α, a key upstream regulator of the SASP (Orjalo et al. 2009; Acosta et al. 2013), and observed substantially reduced IL1α in MLL1 knockdown OIS compared with SC OIS cells (Fig. 1D). Together, these results strongly support our RNA-seq observations that MLL1 reduction attenuates SASP expression.

To confirm that these results were not unique to H-Ras V12-induced fibroblasts, we tested a second model of OIS using primary human melanocytes (in lieu of fibroblasts). The primary melanocytes were induced to enter senescence via a doxycycline-inducible form of the *BRAFV600E* oncogene (diBRAF). This system models the formation of a melanocytic nevus, a well-established example of in vivo OIS (Michaloglou et al. 2005). As with our fibroblast analysis, we examined the top 20 most up-regulated SASP genes in *BRAF*-induced melanocyte OIS by RNA-seq and observed a similar profile of the most highly up-regulated SASP genes as compared with the senescent fibroblasts, including *IL1B*, again the most up-regulated of all genes in the melanocytes (Supplemental Fig. S1H,I). Similar to *HRAS*-induced OIS, previous data suggest that *BRAF*-induced OIS leads to cellular hyperproliferation in vitro and in vivo (Zhu et al. 1998; Dankort et al. 2007) and that in vivo human nevi
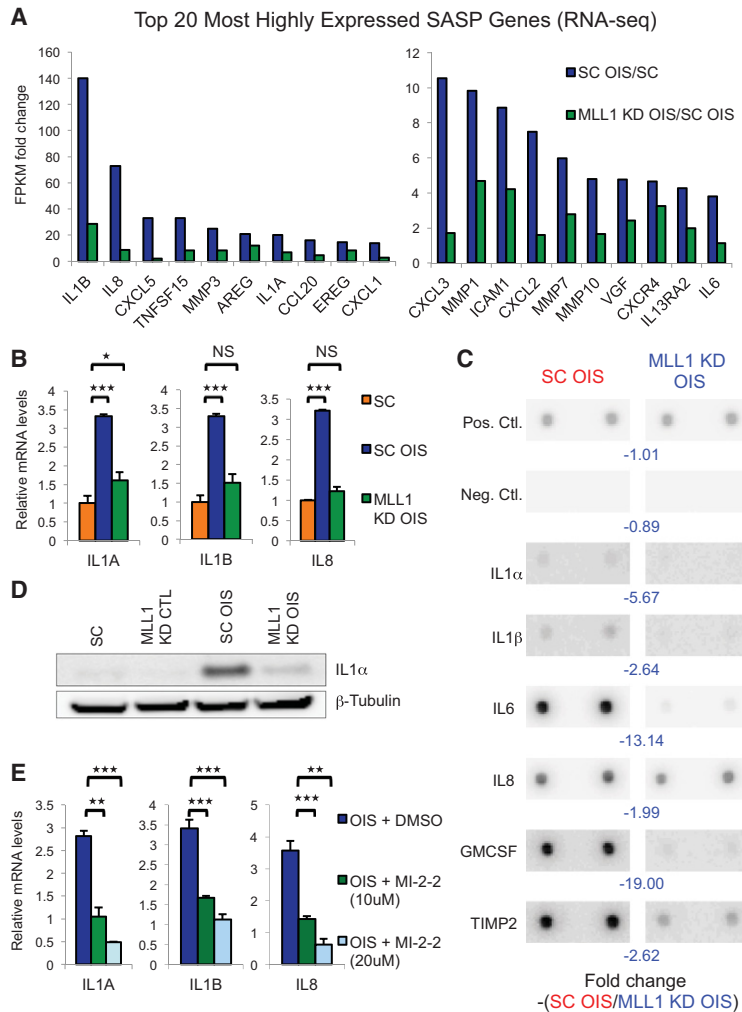
Figure 1. MLL1 inhibition dramatically attenuates SASP expression. (*A*) Genome-wide RNA-seq, displayed here as fold change from control (SC) FPKM (fragments per kilobase per million mapped fragments) values, demonstrates a broad and striking reduction in the top 20 most highly up-regulated SASP genes in MLL1 knockdown (KD) OIS cells (green) as compared with the SC OIS cells (blue). (*B*) RT-qPCR performed in three biological replicates confirms RNA-seq results of some of the most highly expressed SASP genes (comparing MLL1 knockdown OIS cells in green with SC OIS cells in blue). Control "SC" cells are shown in orange. (*C*) An ELISA array for the most highly up-regulated SASP genes displays decreased secretion of all SASP factors in conditioned medium derived from MLL1 knockdown OIS cells in comparison with SC OIS cell-derived conditioned medium. Image density values were calculated by Licor Image Studio Lite and used to calculate the negative fold change [–(SC OIS/MLL1 knockdown OIS)], which is displayed in blue. (*D*) Western blotting demonstrates a significant reduction in protein levels of the key upstream SASP mediator IL1α in MLL1 knockdown OIS cells in comparison with SC OIS cells. (*E*) Pharmacological inhibition of the MLL/Menin interaction with 10 μM MI-2-2 dramatically reduces SASP expression by RT-qPCR in comparison with OIS cells treated with vehicle only (DMSO). Furthermore, treatment with both 10 and 20 μM doses of MI-2-2 demonstrates a dose responsiveness to SASP inhibition. Log values are reported here so that they may be compared on a similar scale.

display features of an activated DDR (Gorgoulis et al. 2005; d'Adda di Fagagna 2008; Sheu et al. 2012). Thus, we performed MLL1 knockdown in diBRAF melanocytes, and, similar to the fibroblast system, this led to a reduction of both MLL1 and SASP gene expression (Supplemental Fig. S1J). As an additional measure of the effect of MLL1 inhibition, we used the commercial pharmacologic MI-2-2, which inhibits MLL1 activity via blocking the interaction between MLL1 and its essential cofactor, Menin (Huang et al. 2012), and such inhibitors display anti-cancer activity in several human tumor types (Borkin et al. 2015; Malik et al. 2015; Zhu et al. 2015). Importantly, pharmacological inhibition of MLL1 activity by MI-2-2 in fibroblasts also abrogated the SASP to the same extent as shRNA-mediated knockdown of MLL1 as measured by RT-qPCR (Fig. 1E). Thus, we confirmed in two OIS models that decreasing MLL1 using shRNA reduction results in reduced SASP expression and that pharmacological inhibition of MLL1 activity similarly abrogated SASP expression. These observations demonstrate that MLL1 inhibition potently reduces SASP expression and suggest that MLL1 has an essential and specific role in the pathway to activate SASP in OIS.

MLL1 inhibition does not alter OIS growth arrest

Given this extensive SASP reduction, we tested whether MLL1 inhibition affects factors required for normal onset or maintenance of OIS. We performed Western blot analysis for the critical OIS tumor suppressor and senescence mediator CDKN2A (p16) in SC, SC OIS, and MLL1 knockdown OIS cells. We did not detect any decrease in p16 or Ras protein expression in MLL1 knockdown OIS cells as compared with SC OIS cells (Fig. 2A). Thus, importantly, in spite of the dramatic reduction in SASP expression by lowering MLL1 levels, neither oncogene expression nor senescence itself was decreased. These observations are consistent with previous findings that expression of *CDKN2A* is primarily controlled by H3K27me3 levels (Bracken et al. 2007; Agger et al. 2009; Barradas et al. 2009). We further confirmed these results with RT-qPCR and RNA-seq and found that CDKN2A mRNA levels were consistently higher in MLL1 knockdown OIS cells compared with SC and SC OIS (Fig. 2B,C). RNA-seq examination of other hallmark senescence genes showed that MLL1 knockdown OIS cells displayed increases in a number of tumor suppressors (*CDKN1A*, *CDKN2A*, and
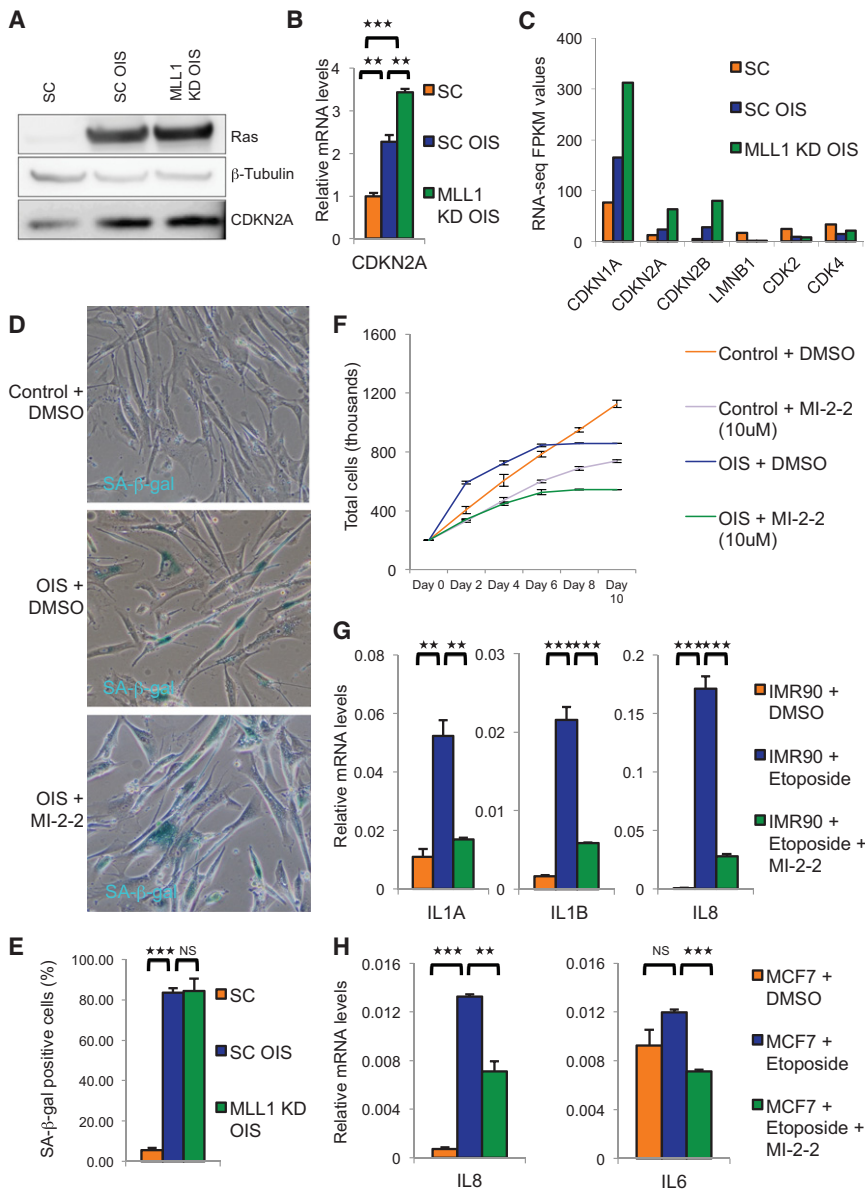
Capell et al.

Figure 2. MLL1 inhibition has no effect on OIS growth arrest and blocks DDR-induced inflammation independently of senescence. (*A*) Western blotting shows that both Ras and CDKN2A/P16 levels are unchanged in MLL1 knockdown (KD) OIS cells in comparison with SC OIS cells. (*B*) RT-qPCR confirms that CDKN2A mRNA levels increase in MLL1 knockdown OIS cells (green) and are higher than those in SC OIS cells (blue). (*C*) RNA-seq demonstrates that MLL1 knockdown OIS cells follow transcriptional patterns typically seen in OIS, including increased levels of tumor suppressors *CDKN1A*, *CDKN2A*, and *CDKN2B* as well as decreases in nuclear lamina component *LMNB1* and cyclin-dependent kinases *CDK2* and *CDK4*. (*D,E*) SA-β-gal staining (*D*) and its quantification (*E*) show that MI-2-2-treated cells express SA-β-gal in percentages similar to those of normal OIS cells treated with DMSO, while control cells do not. (*F*) A growth curve analysis demonstrates that MLL1 inhibition by MI-2-2 slows proliferation in both control and OIS cells and prevents the hyperproliferative period typically seen following oncogene induction during the first 48 h of OIS onset. (*G*) Normal proliferating IMR90 fibroblasts exposed to the DNA-damaging agent etoposide for 48 h are unable to express SASP genes in the setting of a single dose of 10 μM MI-2-2 given at the same time as the etopside, in contrast to DMSO-treated cells. (*H*) MCF7 human breast cancer cells were likewise treated in the same manner with etoposide and similarly were unable to up-regulate inflammatory cytokines.

CDKN2B) and decreases in *LMNB1* and cyclin genes (*CDK2* and *CDK4*) (Fig. 2C) to levels that are typical of senescence in our assays. Importantly, OIS fibroblasts treated with the MLL1/Menin inhibitor MI-2-2 also stained positively for SA-β-gal in percentages similar to those of normal OIS cells (Fig. 2D,E), further arguing against impaired OIS induction or maintenance as an explanation for our findings. We then measured cell proliferation under MLL1 inhibition for both normal and OIS cells. Treatment with 10 μM MI-2-2 repressed cellular proliferation in both normal cells and cells harboring an activated oncogenic HRasV12 (Fig. 2F). These results are consistent with recent evidence using a similar MLL1 inhibitor, MI-503, in MLL1 leukemia cells (Borkin et al. 2015). Intriguingly, while normal OIS cells underwent an initial period of hyperproliferation in the first 48 h upon Ras induction, this effect was not observed in cells treated with MI-2-2 (Fig. 2F). Thus,

MLL1 inhibition strikingly attenuates the SASP while having no effect on the tumor-suppressive growth arrest.

MLL1 inhibition blocks DDR-induced inflammation independently of senescence

We next determined whether MLL1 inhibition might function more broadly to regulate inflammatory gene expression in the contexts of both DNA damage and cancer. Thus, we tested whether MLL1 inhibition would similarly block cytokine and "SASP-like" gene expression following DNA damage, specifically independently of senescence. To do this, we treated normal proliferating fibroblasts with the DNA-damaging chemotherapeutic agent etoposide. Cells exposed to etoposide and harvested after 48 h, prior to the onset of senescence, displayed significant up-regulation of SASP genes such as *IL1A*, *IL1B*,

and *IL8* (Fig. 2G). Importantly, the addition of the MLL1 inhibitor MI-2-2 abrogated this up-regulation of SASP genes (Fig. 2G). Similar results were obtained by repeating this experiment in MCF7 breast cancer cells (which up-regulated SASP genes *IL6* and *IL8* but not *IL1A* or *IL1B* significantly) (Fig. 2H), mimicking the clinical scenario of TIS or DNA damage-induced tumor secretomes (Obenauf et al. 2015). Together, these data indicate that MLL1 inhibition may prevent DNA damage-induced cytokine secretion and inflammation from both normal and cancerous cells independently of senescence.

MLL1 inhibition prevents the procarcinogenic effects of the SASP and represses inflammation in cancer in vivo

We next assessed the functional consequences of MLL1 inhibition on DDR-induced cytokine/SASP expression using a cellular migration assay with conditioned medium

from senescent cells. This assay has been used as a standard measure to assess the functional effects of secreted factors in numerous contexts, including in senescence and cancer, to show the functional effects of secreted factors on premalignant and malignant cells (Jenei et al. 2009; Walter et al. 2010; Yew et al. 2011; Canino et al. 2012; Sun et al. 2012; Justus et al. 2014). Conditioned medium derived from normal SC OIS cells substantially enhanced cellular migration of human MCF7 breast cancer cells after 3 d (Fig. 3A, cf. day 1 and day 4, middle panels). In contrast, conditioned medium derived from MLL1 knockdown OIS cells did not stimulate or differentially affect cellular migration, similar to medium derived from control SC cells (Fig. 3A, cf. top and bottom panels). Image analysis software quantified these results and confirmed the inability of the MLL1 knockdown OIS medium to enhance cancer cell migration (Supplemental Fig. S2A, B). This observation further supports a model in which
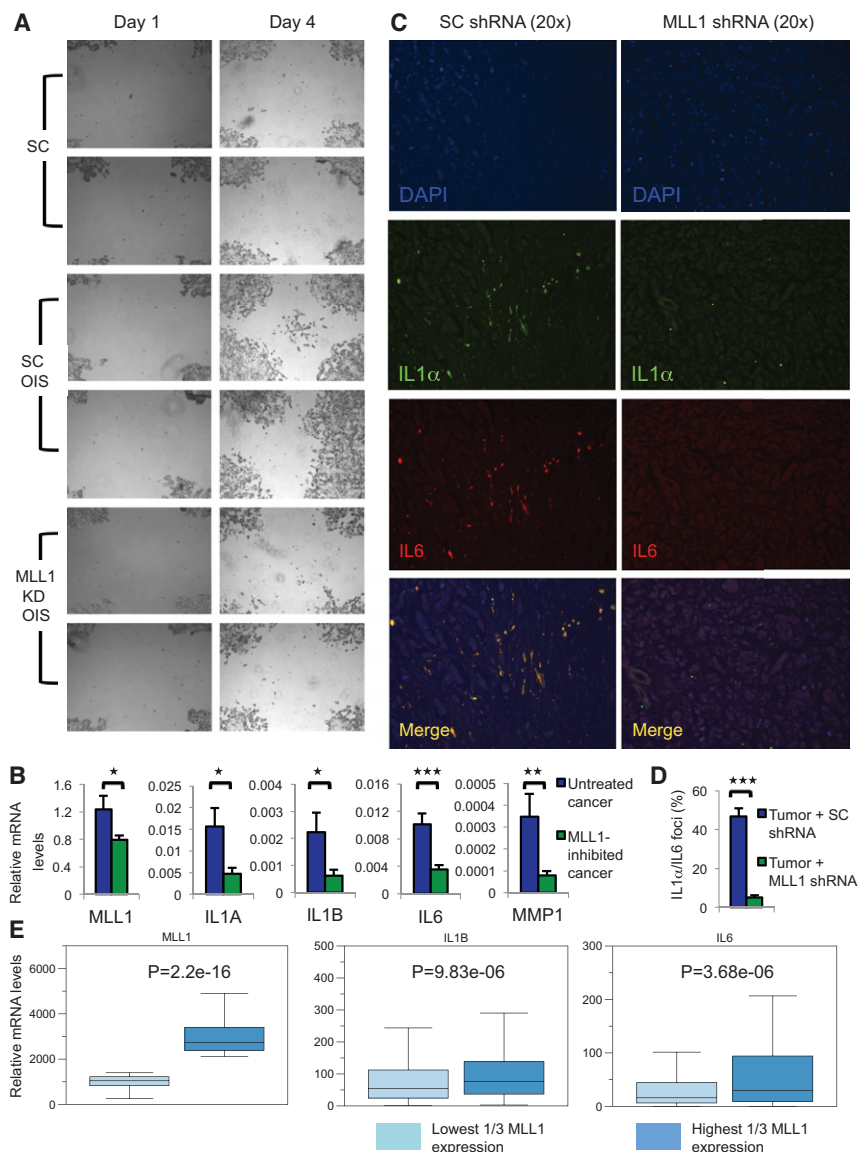

Figure 3. MLL1 inhibition prevents the procarcinogenic effects of the SASP and inhibits inflammation in cancer in vivo. (*A*) Cellular proliferation assay of MCF7 breast cancer cells exposed to conditioned medium from either SC cells (*top* panels), SC OIS cells (*middle* panels), or MLL1 knockdown (KD) OIS cells (*bottom* panels) demonstrates that while SC OIS cell medium containing a normal amount of the secreted SASP leads to enhanced cellular growth and migration of this cancer, the medium derived from the MLL1 knockdown OIS cells does not and is more comparable with the SC cells that have no SASP. (*B*) RT-qPCR of xenograft tumors demonstrates that tumors derived from MLL1 shRNA-treated tumors display significantly less expression of *MLL1*, *IL1A*, *IL1B*, and *IL6* as compared with those tumors derived from SC shRNA treatment. (*C*) Immunofluorescence (IF) (20×) of tumor sections also demonstrates reduced expression of IL1α (green) and IL6 (red) in tumors derived from the MLL1 shRNA-treated tumors as compared with tumors derived from SC shRNA treatment. (*D*) The average of the quantification of three representative 20× IF fields from tumor sections shows that MLL1-inhibited tumors express significantly fewer foci of IL1α and IL6 than SC shRNA-treated tumors. (*E*) An examination of 1215 human breast cancer patient samples from The Cancer Genome Atlas (TCGA) demonstrates that the highest one-third of *MLL1*-expressing tumors have significantly higher SASP expression (*IL1B* and *IL6* shown here) than tumors in the lowest one-third of *MLL1* expression.

MLL1 inhibition can reduce SASP expression and thus prevent the previously described procarcinogenic, proproliferative functions.

MLL1 inhibitors have recently been shown to have antiproliferative and anti-cancer effects in successfully treating mouse models of cancer in vivo (Borkin et al. 2015; Malik et al. 2015; Zhu et al. 2015). However, the effects of MLL1 inhibition on proinflammatory cytokine gene expression in cancer in vivo is unknown. As MI-2-2 does not have in vivo biological activity, in order to answer this question, we performed tumor xenografts. Human breast cancer cells were stably infected with lentivirus encoding either SC or MLL1 shRNAs and injected into mice subcutaneously to allow for tumor formation. The tumors were harvested and subjected to cytokine gene expression analyses. Decreased expression of both *MLL1* and SASP-like cytokine genes, including *IL1A*, *IL1B*, *IL6*, and *MMP1*, were detected by RT-qPCR (Fig. 3B). Protein levels were also reduced, as immunofluorescence (IF) assays demonstrated repressed levels of IL1α and IL6 (Fig. 3C; Supplemental Fig. S2D). IL1α and IL6 colocalized, and quantification of IL1α/IL6 foci in multiple 20× fields confirmed decreased levels of SASP expression (Fig. 3D). Together, these results suggest that inhibiting MLL1 in vivo can decrease SASP-like inflammatory gene expression and suggest a possible additional novel mechanism by which MLL1 inhibition is effective for cancers in vivo (Borkin et al. 2015; Malik et al. 2015).

Next, we analyzed clinical tumor samples from human breast cancers using The Cancer Genome Atlas (TCGA). Examining all samples (1215) and extracting those with both the highest and lowest one-third of *MLL1* expression, we observed a significant positive correlation between high *MLL1* expression and high SASP gene expression, including *IL1A*, *IL1B*, *IL6*, and *IL8* (Fig. 3E; Supplemental Fig. S3A, with corresponding *P*-values), which was not evident for control housekeeping genes such as *GAPDH*, *ACTB*, and *LMNA* (Supplemental Fig. S3A). We then examined another common human cancer, prostate cancer (551 total samples), and found similar positive correlations, as patient tumor samples with the highest expression of *MLL1* also had significantly higher levels of SASP gene expression, including *IL1A*, *IL1B*, and *IL8* (Supplemental Fig. S3B, with *P*-values included). These trends were also not present for control housekeeping genes, including *ACTB*, *GAPDH*, and *LMNA* (Supplemental Fig. S3B). Together, these results demonstrate that MLL1 inhibition prevents the expression of these SASP-like inflammatory genes in vivo in human cancer xenografts and are further supported by our discovery of a novel in vivo correlation between MLL1 and SASP gene expression in human patient cancer samples.

MLL1 inhibition leads to greater losses of γH2A.X than H3K4me3 enrichment over SASP genes

To further assess the epigenomic effect of MLL1 on the SASP, we performed ChIP-seq (chromatin immunoprecipitation [ChIP] combined with deep sequencing) for H3K4me3 and γH2A.X. MLL1 deposits H3K4me3 at tran-

scriptional start sites (TSSs) (Rao and Dou 2015), and an activated DDR leads to the phosphorylation of the histone variant H2A.X (called γH2A.X) that occurs surrounding sites of DNA breaks (Rogakou et al. 1999). We performed ChIP-seq for H3K4me3 and γH2A.X in control (both CTL and SC cells), normal OIS (as well as SC OIS), and MLL1 knockdown OIS cells using either Hi-Seq or NextSeq platforms using total histone and input as controls. We found that the most highly up-regulated SASP genes by RNA-seq, such as *MMP1* and *IL1B*, displayed extensive increases in both H3K4me3 and γH2A.X binding during OIS (Fig. 4A; Supplemental Fig. S4A). Indeed, when the top 1% most highly expressed genes in OIS were plotted by levels of expression (as measured by RNA-seq) and γH2A.X (as measured by ChIP-seq) and colored by levels of H3K4me3 (Supplemental Fig. S4B, in red), SASP genes displayed some of the largest increases in these measures in OIS (Supplemental Fig. S4B, SASP genes highlighted within the red box). Intriguingly, rather than broad megabase domains of γH2A.X, as typically observed adjacent to DNA double-strand breaks (Rogakou et al. 1999), the increases over the SASP genes were extensive yet restricted to gene bodies (Fig. 4A; Supplemental Fig. S4A). We note that this novel observation of dramatic gene body enrichment in γH2A.X was similarly observed recently in association with neuronal response genes undergoing rapid activation (Madabhushi et al. 2015). Future investigations will likely determine the function of γH2A.X in this setting.

We next determined the effect of MLL1 depletion on these chromatin changes. H3K4me3 ChIP-seq in MLL1 knockdown OIS cells demonstrated that some SASP genes have reduced H3K4me3, including *MMP1*, *MMP10*, *SERPINB2*, *CXCL3*, and *CCL3* (Fig. 4B). However, the overall loss of H3K4me3 enrichment was modest and did not correspond well to the dramatic decreases in transcription of the SASP (*P* = 0.42), as some prominently repressed genes did not lose any H3K4me3, such as *IL1A* and *IL1B* (Fig. 4B,C). In contrast, decreases in gene body γH2A.X in MLL1 knockdown OIS were more extensive and were detected for almost all down-regulated SASP genes (*P* = 0.02; Fig. 4B), including *MMP1* as a clear example (Fig. 4D). Together, these ChIP-seq data suggest that the most up-regulated SASP genes possess a consistent epigenetic signature marked by large enrichment of both H3K4me3 and γH2A.X in OIS. Importantly, though, the effects of MLL1 inhibition did not correlate strongly to reductions in H3K4me3 enrichment at SASP genes but rather, apparently, through an independent effect on DDR signaling to the SASP genes, as reflected in a consistent decrease in γH2A.X enrichment.

MLL1 inhibition in OIS prevents activation of the ATM–NF-κB signaling axis

We reasoned that MLL1 might have a direct effect on the DDR, which then potentially manifests in the changes that we observed in SASP gene expression. To test this, we first examined whether MLL1 inhibition altered activation of the DDR. We performed RT-qPCR for ATM,
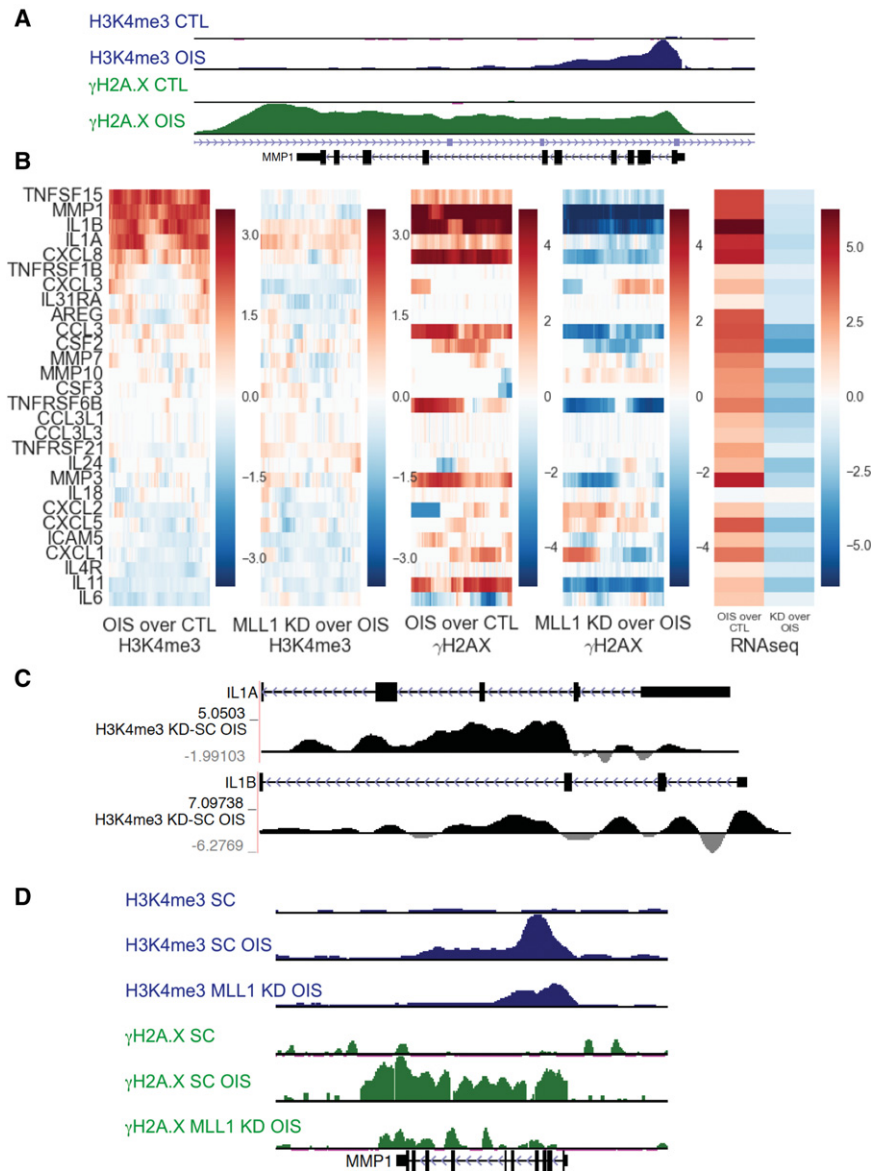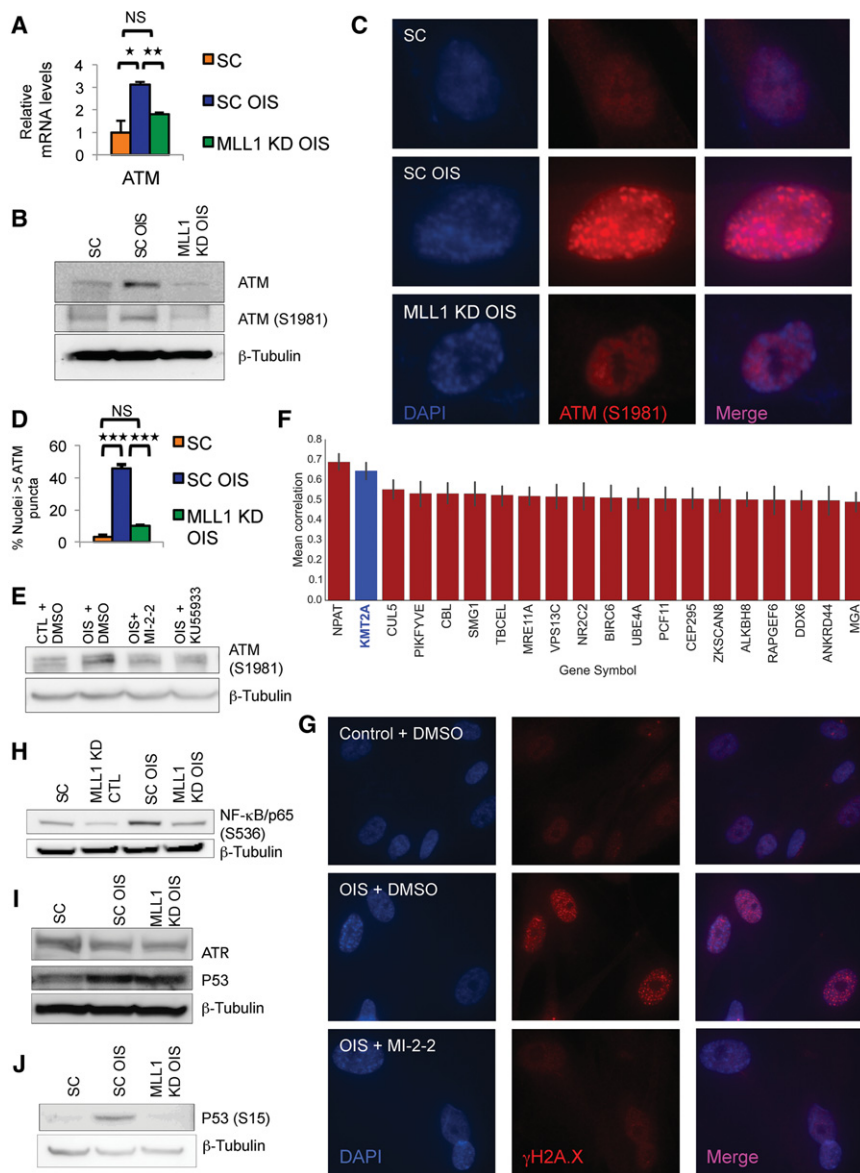
Figure 4. MLL1 inhibition leads to greater losses of γH2A.X than H3K4me3 enrichment over SASP genes. (*A*) ChIP-seq tracks display dramatic increases in H3K4me3 (blue) over SASP gene promoters and γH2A.X (green) over SASP gene bodies in OIS as compared with control proliferating cells (CTL), as seen here over the SASP gene *MMP1*. (*B*) Heat map based on ChIP-seq (first through fourth columns) and RNA-seq (fifth column) of SC, SC OIS, and MLL1 knockdown (KD) OIS cells of all SASP genes demonstrates that many, but not all, SASP genes gain H3K4me3 (as measured over the promoter and TSS) in the transition from proliferating SC cells to OIS (SC OIS) (first column). When comparing H3K4me3 levels by ChIP-seq between SC OIS cells and MLL1 knockdown OIS cells (second column), some SASP genes lose H3K4me3 enrichment in MLL1 knockdown OIS cells, although the changes are not uniform and do not correlate well with expression changes. In contrast, almost all SASP genes demonstrate both increases in γH2A.X enrichment (as measured over the gene body) going from the control (SC) to the OIS (SC OIS) state (third column) as well as decreases in γH2A.X enrichment with MLL1 knockdown in OIS (MLL1 knockdown OIS) (fourth column). (*C*) Delta track of H3K4me3 ChIP-seq data (MLL1 knockdown OIS/SC OIS) demonstrates representative SASP genes (*IL1A* and *IL1B*) that, despite decreasing extensively in expression with MLL1 knockdown, do not lose, but rather actually gain, H3K4me3 enrichment with MLL1 knockdown. (*D*) ChIP-seq track views over a representative SASP gene (*MMP1*) display modest decreases in promoter H3K4me3 levels but more extensive losses in gene body γH2A.X levels in MLL1 knockdown OIS cells as compared with SC OIS cells. SC proliferating cell tracks are labeled as SC here.

which is essential for SASP activation (Rodier et al. 2009) and phosphorylates the key SASP transcription factor NF-κB p65 (phospho-S536) (Piret et al. 1999; Huang et al. 2003; Wu et al. 2006). We observed significant reduction of ATM mRNA levels in MLL1 knockdown OIS cells compared with SC OIS cells (Fig. 5A). Western blotting likewise demonstrated decreased levels of total ATM protein, including its activated form, ATM phospho-S1981 (Fig. 5B). To visualize this loss of ATM in cells, we performed IF for ATM phospho-S1981 in MLL1 knockdown OIS cells as compared with normal SC and SC OIS cells and quantified positively staining nuclear puncta. MLL1 knockdown OIS cells consistently displayed significantly reduced numbers of ATM phospho-S1981 nuclear puncta in comparison with SC OIS cells (Fig. 5C,D; Supplemental Fig. S4C). We also performed Western blotting for ATM phospho-S1981 using control or OIS cells treated

with MI-2-2. Similar to MLL1 shRNA treatment, we observed reduced ATM phospho-S1981 in OIS cells treated with MI-2-2 to levels seen in control proliferating cells (Fig. 5E). As a control, this reduction was similar to the effect of a specific inhibitor of phospho-ATM (KU55933) on OIS cells (Fig. 5E), which also effectively inhibited the SASP genes *IL1A*, *IL1B*, and *IL8* (Supplemental Fig. S4D; Rodier et al. 2009).

We examined this relationship between ATM expression and MLL1 further by looking at clinical tumor samples from TCGA (Cerami et al. 2012; Gao et al. 2013). Similar to SASP genes as described above (Fig. 3E; Supplemental Fig. S3A,B), tumors with the highest levels of MLL1, also displayed significantly higher levels of ATM (Supplemental Fig. S3A,B). Remarkably, upon closer examination, we observed that *MLL1* was among the most highly coexpressed genes with *ATM* in each type of human

Capell et al.

Figure 5. MLL1 inhibition in OIS prevents activation of the ATM–NF-κB signaling axis. (*A*) ATM mRNA expression is reduced in OIS cells treated with MLL1 shRNA (MLL1 knockdown [KD] OIS; green) as compared with SC OIS cells (blue) as measured by RT-qPCR. SC proliferating cells are in orange. (*B*) Western blotting shows that MLL1 knockdown OIS cells have reduced levels of both total ATM and activated ATM (phospho-S1981) in comparison with SC OIS cells. (*C*) IF of MLL1 knockdown OIS cells displays decreased activated ATM (phospho-S1981) nuclear puncta (red) in MLL1 knockdown OIS cells as compared with SC OIS cells. Blue staining indicates DAPI-stained DNA, while pink staining represents the merged image. (*D*) Quantification of the percentage of cells in SC, SC OIS, and MLL1 knockdown OIS cells with at least five positively staining red nuclear puncta by IF demonstrates a significant reduction in MLL1 knockdown OIS cells. SC OIS compared with SC, *P*-value = 0.0015; MLL1 knockdown OIS compared with SC OIS, *P* = 0.0068. (*E*) ATM (phospho-S1981) protein levels are also reduced by pharmacological treatment with a MLL1/Menin interaction inhibitor, MI-2-2 (10 μM), which prevents its H3K4me3 activity and is similar in efficacy to a targeted inhibitor of phospho-ATM, KU55933 (10 μM). (*F*) Ranking of the top 20 genes that correlate with *ATM* expression across all human cancers in TCGA demonstrates that *MLL1* is the second most highly correlated gene from the entire genome across all tested cancers, second only to *NPAT*, which shares a bidirectional promoter with *ATM*, and ahead of genes with known functional relationships with ATM (*SMG1* and *MRE11A*). (*G*) IF of OIS cells treated with MI-2-2 displays reduced foci of the DNA damage marker γH2A.X as compared with DMSO-treated OIS cells. (*H*) NF-κB p65 (phospho-S536), which is downstream from activation of ATM and is a critical SASP transcription factor, was decreased in MLL1 knockdown OIS cells in comparison with SC OIS cells. (*I*) MLL1 knockdown OIS cells display no differences in total ATR or P53 levels from normal SC OIS cells, suggesting that the effects of MLL1 inhibition are more specific for the ATM-mediated arm of the DDR and not just a global inhibition of the DDR. (*J*) Consistent with repressed activation of ATM, which phosphorylates P53, P53 (phospho-S15) is decreased in MLL1 knockdown OIS cells as compared with normal SC OIS cells.

cancer examined for which RNA-seq expression data were available (Supplemental Fig. S5A). For example, comparing 20,444 genes ranked from 1098 invasive breast cancer samples, *MLL1* was the second most highly coexpressed gene with *ATM* (Pearson's correlation, 0.77) (Supplemental Fig. S5B; Cerami et al. 2012; Gao et al. 2013). This strong positive correlation held for each of the 24 cancer types analyzed. Global analysis combining data from all 24 TCGA cancer types showed that *MLL1* is the second most highly coexpressed gene with *ATM* across all cancer types (Fig. 5F; Supplemental Fig. S5C). *MLL1* coexpression with *ATM* was higher than several genes with known

functional relationships with ATM in the DDR, including *MRE11A* and *SMG1* (Fig. 5F). Notably, the only gene that was more highly coexpressed with *ATM* than *MLL1* was *NPAT*, which shares a bidirectional promoter with *ATM* (Fig. 5F; Imai et al. 1996). The robustness of the observed correlation between *MLL1* and *ATM* mRNA abundance in such a large and diverse set of human cancers in vivo is supportive of this potential functional relationship that we observed here with MLL1 in vitro.

Consistent with the decreased levels of chromatin-bound γH2A.X observed in the ChIP-seq data as well as with the failure of ATM activation, MI-2-2 also displayed

reduced levels of nuclear γH2A.X foci by IF, a standard measure of DNA damage (Fig. 5G). Furthermore, the SASP transcription factor NF-κB p65 (phospho-S536) was also decreased to levels seen in SC cells (Fig. 5H). To assess the specificity of this effect on ATM, we assayed total levels of other DDR effectors, ATR and p53. Total ATR levels were decreased in both SC OIS and MLL1 knockdown OIS, consistent with cells that are no longer replicating (Fig. 5I). Total p53 was likewise unchanged between SC OIS and MLL1 knockdown OIS cells (Fig. 5I). In contrast to total p53 levels and consistent with decreased levels of ATM phospho-S1981, p53 phospho-S15, known to be phosphorylated by activated ATM, was decreased in MLL1 knockdown OIS cells as compared with SC OIS cells (Fig. 5J). Taken together with our other observations, our results demonstrate that both genetic inhibition and pharmacologic inhibition of MLL1 level and activity significantly reduce ATM-mediated DDR signaling, a required upstream regulator of SASP expression.

MLL1 directly regulates the expression of numerous critical proproliferative cell cycle regulators and cancer target genes

Since the dramatic attenuation of SASP expression with MLL1 inhibition did not correspond to statistically significantly reduced levels of H3K4me3 at SASP gene promoters, we looked more closely at the genes that were significantly losing H3K4me3 with MLL1 reduction. We performed GO analysis of the top 500 genes exhibiting the greatest loss of H3K4me3 enrichment by ChIP-seq in MLL1 knockdown OIS cells as compared with SC OIS cells. This revealed gene categories enriched for critical kinases and transcription factors required for both cell cycle progression and checkpoint cascades, including activation of the DDR (fold enrichment > 5, $P < 0.05$) (Supplemental Fig. S6A; Di Micco et al. 2006; Cerqueira et al. 2009; Tian et al. 2009; Johnson and Shapiro 2010; Liu et al. 2010; Shintomi et al. 2015; Sivakumar and Gorbsky 2015). These genes, including *AURKA*, *AURKB*, *BIRC5*, *CCNA2*, *CCNB2*, *CCNB1*, *CDC20*, *CDK1*, *CDK2*, *CHEK1*, *FOXM1*, *KIF20A*, *MAD2L1*, *NCAPG*, Polo-like kinase 1 (*PLK1*), *TOP2A*, and *UBE2C* (examples displayed in Fig. 6A; Supplemental Fig. S6B–G), exhibited more extensive losses of H3K4me3 (average loss of −0.657) than even the Hox genes (average loss of −0.077), which MLL1 is well known to regulate (Milne et al. 2002). Notably, many of these proproliferative genes, including Survivin (*BIRC5*), Aurora kinases (*AURKA* and *AURKB*), *PLK1*, *FOXM1*, and *CDC20*, are currently being targeted for pharmacological reduction in a diverse array of cancers, as their high expression in patient tumor samples correlates with worse survival (Gentles et al. 2015). When all genes in the genome were plotted according to levels of expression and H3K4me3, these proproliferative cell cycle genes had clear reductions in expression ($P = 0.02$) that corresponded with their losses of H3K4me3 enrichment with MLL1 knockdown in OIS ($P = 7.0 \times 10^{-8}$), in striking contrast to SASP genes, which did not uniformly lose H3K4me3 (Fig. 6B).

These observations suggest that MLL1 may be critical for direct normal regulation of an array of proproliferative cell cycle genes that have been implicated in cancer. We examined whether MLL1 knockdown also reduced the expression of these genes independently of senescence using RNA-seq on normal proliferating fibroblasts treated with MLL1 shRNA (MLL1 knockdown CTL). GO analysis of the top 500 down-regulated genes in MLL1 knockdown CTL cells compared with SC cells again demonstrated a strong enrichment of the same proproliferative cell cycle regulators (fold enrichment > 5, $P < 0.05$) (representative genes displayed in Fig. 6C; Supplemental Fig. S6H). Indeed, the intersection of all genes that were in the top 500 genes with maximum H3K4me3 reduction by ChIP-seq with MLL1 knockdown in OIS and the top 500 genes with the maximum reduced expression by RNA-seq with MLL1 knockdown in normal proliferating cells (MLL1 knockdown CTL) identified 57 genes ($P = 3.4 \times 10^{-53}$) for which MLL1 likely has a direct role in regulating their expression through H3K4me3 (Fig. 6D).

To directly test the role of MLL1 in the regulation of these proproliferative cell cycle genes, we overexpressed *MLL1* in cells that were simultaneously treated with MI-2-2, hypothesizing that strongly increasing MLL1 levels could potentially rescue the loss of expression of these proproliferative cell cycle genes caused by MI-2-2. Normal fibroblasts were treated with a single dose of 10 μM MI-2-2, simultaneously transfected with either empty or MLL1 overexpression plasmids, and harvested 48 h later for mRNA analysis. As a control for transfection efficiency, transfecting GFP into the same IMR90 fibroblasts demonstrates that >80% of cells show GFP positivity (Supplemental Fig. S6I,J). RT-qPCR results demonstrated that transfection by the *MLL1* overexpression plasmid did result in a striking up-regulation of MLL1 mRNA by >10,000-fold (Fig. 7A). Subsequent RT-qPCR of key proproliferative cell cycle genes showed partial to complete rescue of mRNA expression levels (Fig. 7B), suggesting that the dramatic up-regulation of MLL1 simply overwhelmed the capacity of the single MI-2-2 dose to fully inhibit MLL1 activity and allowed for the continued expression of these proproliferative cell cycle genes. Combined with the above RNA-seq and ChIP-seq results as well as previous data demonstrating a direct role for MLL1 in controlling the expression of a subset of cyclin genes (Takeda et al. 2006), this observation is highly supportive of MLL1 having a direct role in the expression of these proproliferative cell cycle genes.

Next, we examined the expression of these proproliferative cell cycle genes 48 h after oncogene activation during the period of hyperreplication and prior to the onset of OIS. MLL1 has been shown to be critical for progression of S phase, and inhibition of normal S-phase replication and checkpoint function impairs activation of the DDR, including in OIS, where cells must first undergo a period of hyperreplication to trigger the DDR (Di Micco et al. 2006; Cerqueira et al. 2009; Tian et al. 2009; Johnson and Shapiro 2010; Liu et al. 2010)—hence our reasoning for performing this analysis at 48 h after oncogene induction. Strikingly, the RT-qPCR results showed that MLL1
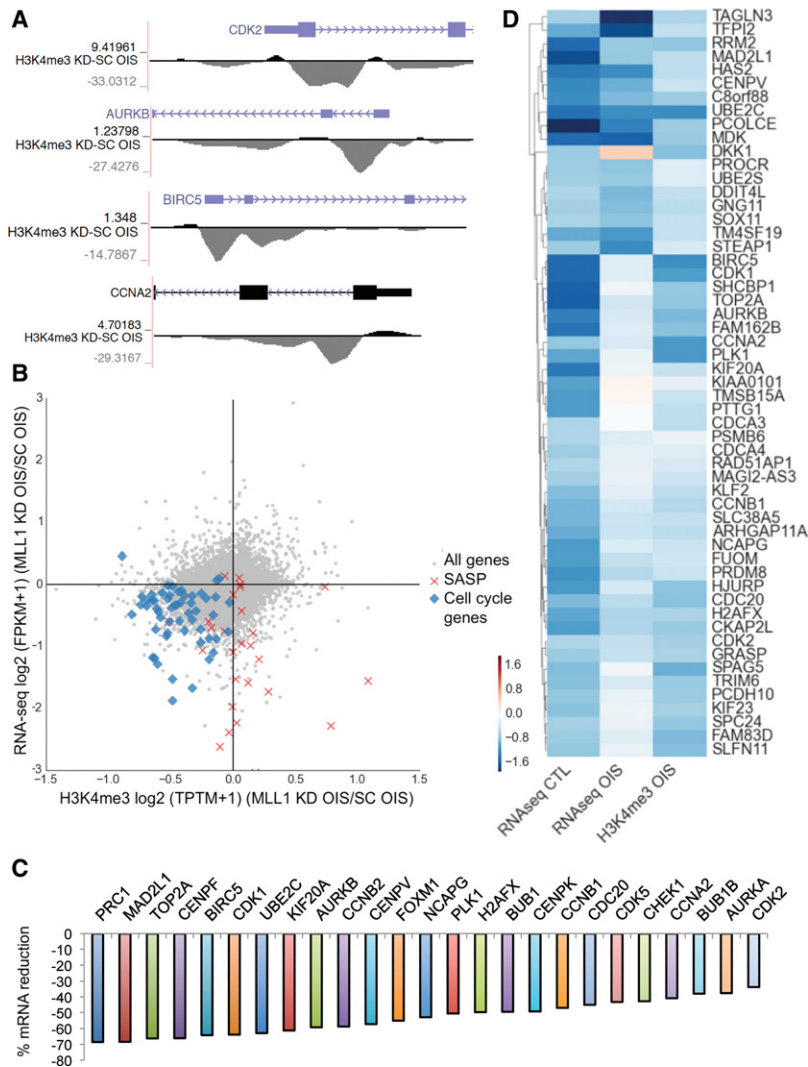
Figure 6. MLL1 directly regulates the expression of numerous critical proproliferative cell cycle and cancer target genes. (*A*) ChIP-seq delta track (MLL1 knockdown [KD] OIS/SC OIS) of H3K4me3 enrichment at the genes *CDK2*, *AURKB*, *BIRC5*, and *CCNA2* demonstrates extensive losses of H3K4me3 at the promoter of both genes in MLL1 knockdown OIS cells. (*B*) Scatter plot of the log ratio of H3K4me3 enrichment (ChIP-seq) and gene expression (RNA-seq) of MLL1 knockdown OIS/SC OIS demonstrates that proproliferative cell cycle and cancer target genes (blue dots) lose both expression and H3K4me3 enrichment in comparison with SASP genes (red Xs) and all other genes (gray dots). (*C*) RNA-seq of MLL1 knockdown in normal control proliferating IMR90s (MLL1 knockdown CTL) in comparison with SC cells demonstrates extensive loss of expression of key proproliferative cell cycle and cancer target genes (genes derived from the top 500 genes that lost expression genome-wide, displayed as the percentage of expression lost with MLL1 knockdown). (*D*) The relative levels of change for the 57 genes that were identified from the intersection of the top 500 genes with the most decreased H3K4me3 enrichment (ChIP-seq) in MLL1 knockdown in OIS cells (MLL1 knockdown OIS) as well as the top 500 genes with the most reduced expression (RNA-seq) with MLL1 knockdown in control cells (MLL1 knockdown CTL) are displayed in heat map form. The first column displays the fold change of loss of expression in control cells with MLL1 knockdown by RNA-seq. The second column displays the loss of expression in OIS cells with MLL1 knockdown by RNA-seq. The third column displays the loss of H3K4me3 in OIS cells with MLL1 knockdown by ChIP-seq. Relative change of H3K4me3 over ±1 kb of the TSS is shown. Euclidean distance with ward metric hierarchical clustering was used.

knockdown OIS cells significantly down-regulated the expression of all tested proproliferative cell cycle genes below the levels seen in SC OIS (Fig. 7C). In fact, while *CDK2* levels were higher in SC OIS cells than proliferating SC cells 48 h after oncogene activation, levels in MLL1 knockdown OIS cells were significantly reduced below both SC and SC OIS cells (Fig. 7C). Taken with our other results, this up-regulation likely occurs through the modification of H3K4me3. Finally, we arrested cells in G1 phase through serum starvation and then treated them with the DNA-damaging agent etoposide. Strikingly, and consistent with previous results (Di Micco et al. 2006), cells arrested in G1 were unable to activate the DDR and induce inflammatory cytokines, including *IL1A*, *IL1B*, *IL6*, and *MMP1* (Fig. 7D). Thus, reduction of MLL1 expression or activity prevents DDR activation and SASP expression through its direct inhibition of the expression of key genes necessary for proliferation, orderly cell cycle progression, and triggering of the DDR (Fig. 7E). Specifically, in contrast to normal OIS cells, MLL1-inhibited cells are unable to have a normal progression through

the S-phase checkpoint due to the reduced expression of proproliferative cell cycle genes and MLL1's known required role for normal S-phase progression (Liu et al. 2010). In turn, these cells are unable to trigger the activation of the DDR and its key mediator for expression of the SASP, ATM phospho-S1981. In contrast, tumor-suppressive cell cycle genes that promote growth arrest, such as CDKN1A and CDKN2A, remain elevated. Together, this demonstrates how MLL1 inhibition enables direct senescence growth arrest without induction of the SASP gene network.

Discussion

In this study, we identified a novel functional relationship between the chromatin regulator MLL1 and an array of proproliferative cell cycle and cancer target genes that control both proliferation and normal DDR engagement. In our key observation, inhibition of MLL1 expression or activity abrogates DDR-induced inflammatory cytokine gene expression in senescence (the SASP) and in
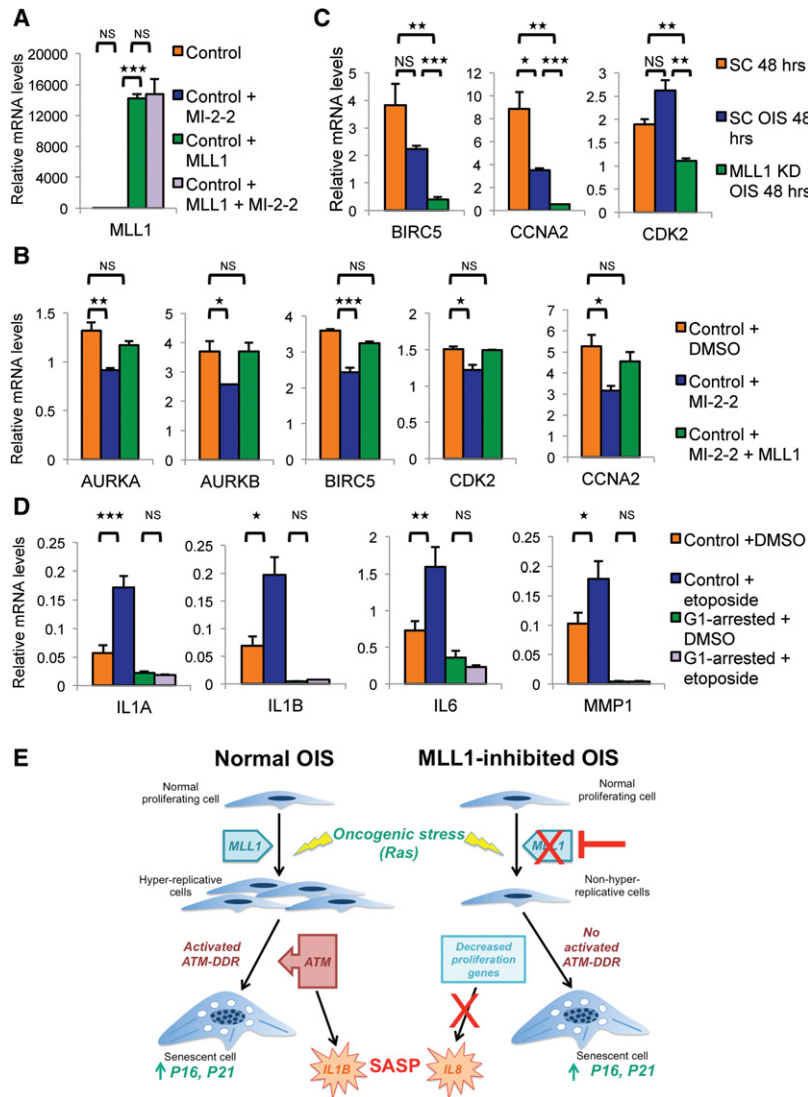
Figure 7. (A) MLL1 overexpression by transient transfection over 48 h demonstrates significant up-regulation by >10,000-fold of *MLL1* by RT-qPCR as compared with vector control transfection. Notably, 10 µM MI-2-2 treatment has no effect on levels of *MLL1*. (B) Normal control IMR90 cells were transfected with either a vector control or *MLL1* overexpression plasmid in the setting of either a single dose of DMSO or 10 µM MI-2-2. After 48 h, RT-qPCR was performed and demonstrated that MLL1 overexpression either partially or fully rescued the expression of proproliferative cell cycle genes *AURKA*, *AURKB*, *BIRC5*, *CCNA2*, and *CDK2*, suggesting that MLL1 has a direct role in regulating their expression. (C) Examination of the expression of proproliferative cell cycle genes 48 h after induction of OIS by RT-qPCR demonstrates that MLL1 knockdown (KD) OIS cells have dramatically decreased levels of mRNA of these genes after just 48 h, even in comparison with SC OIS cells. This 48-h period reflects the early hyperproliferative and hyperreplicative phase prior to OIS onset that is required for DDR activation. Consistent with this, *CDK2* is actually elevated at this time in SC OIS cells in comparison with SC cells but is significantly decreased already in MLL1 knockdown OIS cells. (D) Cells arrested in G1 phase by serum starvation are unable to up-regulate SASP-like inflammatory genes when exposed to DNA-damaging chemotherapy such as etoposide, consistent with previous data showing that S phase is required in order to activate the DDR (Di Micco et al. 2006). (E) Schematic representation of how MLL1 inhibition (*right* side) blocks SASP expression by directly inhibiting the expression of numerous proproliferative cell cycle genes, thus preventing the required hyperproliferative and hyperreplicative phase necessary for activation of the ATM-mediated DDR and its resulting SASP, in comparison with normal OIS cells (*left* side). Despite this lack of DDR, MLL1-inhibited cells still undergo normal tumor-suppressive growth arrest.

chemotherapy-induced DNA damage independently of senescence. Blockade of MLL1 also prevents the ability of the SASP to promote the protumorigenic potential of surrounding cancer cells and, importantly, similarly represses inflammatory gene expression in cancer in vivo. Remarkably, despite the strong attenuation of activated ATM-mediated and NF-κB-mediated SASP expression, the elevation of tumor suppressors such as p16 and p21 and the senescence growth arrest itself are unaffected. This mechanistic uncoupling suggests a possible therapeutic role for MLL inhibition in inducing cancerous growth arrest without the deleterious effects of drug resistance and tumor progression caused by the SASP or chemotherapy-related tumor inflammation.

Although MLL1 has previously been shown to associate with mitotic chromatin (Blobel et al. 2009) and regulate A- and B-type cyclins (Takeda et al. 2006), our data demonstrate that the crucial epigenetic regulatory role of MLL1 may be much broader and may extend to the expression of numerous cancer-promoting kinases and transcription factors such as Aurora kinases (*AURKA* and *AURKB*), Survivin (*BIRC5*), *PLK1*, and *FOXM1*. MLL1 inhibition strongly lowers the expression of these genes, which is likely the direct effect of the inhibitors on the cessation of cell growth, and prevents the critical hyperreplicative S-phase-dependent activation of the DDR. Beyond MLL1's direct chromatin effects on these proliferation-promoting genes, inflammation has been shown to be a "hallmark of cancer" (Hanahan and Weinberg 2011), and the SASP has been shown to enable aspects of tumor progression through the induction of angiogenesis (Coppe et al. 2006), epithelial–mesenchymal transition (EMT) (Laberge et al. 2012), and the promotion of cancer stem-like cells (Cahu et al. 2012). Thus, our findings provide further rationale for testing MLL1 inhibitors as either mono-therapy or adjuvant therapy in other cancers beyond those recently shown to be responsive to MLL1 inhibition (Borkin et al. 2015; Malik et al. 2015; Zhu et al. 2015).

Materials and methods

Cell culture

IMR90 cells (obtained from Coriell Institute for Medical Research) were grown in DMEM without phenol with 10% FBS and 1% penicillin/streptomycin at 3% oxygen. The cells were generated by retrovirally infecting normal IMR90 fibroblasts with pLNCX-ER:Ras, and senescence was induced with 4-OHT (Sigma-Aldrich). MCF7 breast cancer cells (obtained from Coriell Institute for Medical Research) were grown in DMEM with 10% FBS and 1% penicillin/streptomycin at 20% oxygen. Primary human melanocytes were obtained from normal human foreskin. After an overnight incubation in dispase, the epidermis was separated from the dermis and treated with trypsin for 10 min. Cells were pelleted and plated on selective MC Medium 254 (Gibco) with human melanocyte growth supplement and 1% penicillin/streptomycin. Doxycycline (hyclate) hydrochloride (Sigma-Aldrich) was dissolved in sterile, deionized water. Senescent cells were maintained in dishes for 10 d to ensure growth termination. Senescence was determined by monitoring CDKN2A/P16 up-regulation and down-regulation of cyclin genes and by SA-β-gal (Chemicon International). To arrest cells in G1 phase, serum starvation experiments were performed by allowing cells to reach confluency and then removing serum for 4 d prior to harvesting the cells for RNA.

Viral transfection and transduction

diBRAF melanocytes were generated by inserting the human *BRAFV600E* gene immediately after the TetO operator in a modified version of the doxycycline-inducible lentiviral pTRIPZ vector (Thermo Scientific) in which the shRNA hairpin sequences were deleted. HEK293T cells were then seeded at 70% confluency onto six-well plates and incubated in DMEM with 5% FBS and 1% antibiotic and anti-mycotic. Lentiviral plasmid (1.22 µg) was mixed with packaging plasmids pCMVΔR8.91 (0.915 µg) and pUC-MDG (0.305 µg). Plasmids were then mixed with 96 µL of DMEM and 7.2 µL of Fugene6 transfection reagent (Promega) and incubated for 15 min at room temperature. The plasmid solution was then added to the cell medium. Sodium butyrate (10 mM) was added after 16 h, and the cell growth medium was replaced after 24 h and incubated at 32°C. Viral supernatant was collected 45 h after transfection and filtered using a 0.45-µm syringe filter (Argos). Melanocytes seeded at 2.5×10^5 cells per well were incubated in the viral supernatant in the presence of 5 µg mL^{-1} polybrene and centrifuged at 300g for 60 min at room temperature. Cells were then incubated for 15 min at 37°C followed by removal of the viral supernatant and replacement with complete growth medium. For the MLL1 knockdown experiments, MLL1 and SC shRNAs were generously donated from the Hua laboratory at the University of Pennsylvania (http://www.afcri.upenn.edu/ourfaculty/hua_lab.html). Two MLL1 shRNAs were used: MLL1 shRNA 12 (TTAAATTAGGATAATACCGCG) and MLL1 shRNA 14 (AATTATGGTCAAGTGAAGGCG). For the viral transfections, melanocytes and IMR90 fibroblasts were infected with virus at 60% confluency on 10-cm^2 plates for 24 h in the presence of polybrene. Forty-eight hours following infections, cells underwent selection with puromycin to obtain completely puromycin-resistant cell populations. For MLL1 overexpression studies, we used Flag-tagged MLL1-pCXN2, which was a kind gift from Paolo Sassone-Corsi and has been described before (Katada and Sassone-Corsi 2010). Flag-tagged MLL1-pCXN2 (4 µg) and GFP (2 µg) were transfected into IMR90 fibroblasts using Continuum transfection reagent (Gemini Bio-Products) according to the manufacturer's protocol at the same time as MI-2-2 and were harvested for RNA analyses 48 h later.

Migration assay

MCF7 breast cancer cells were grown to confluency. Next, uniform cross-shaped "wounds" were created with a pipet tip. Cells were photographed on day 1 and then incubated with conditioned medium derived from either SC, SC OIS, or MLL1 knockdown OIS cells. Conditioned medium was taken from day 10 serum-free medium that was filtered, and cells were counted to ensure equal dosing of conditioned medium. Cell medium was changed on day 2 with fresh conditioned medium, and cells were then imaged on day 4. For image analysis, images were loaded into a numpy matrix using numpy-1.10.1. The inverse of the luminance of the images was calculated using scikit-image-0.11.3. Values greater than the mean +1 standard deviation for each image were retained and appeared to give accurate representations of cell density. The sum of the inverse luminance was used as a metric of cell count. The difference of this value was calculated between images.

ELISA array

Conditioned medium from two biological replicates harvested as described above was incubated overnight on a RayBio C-Series human inflammation antibody array (RayBiotech) following the manufacturer's protocol. Arrays were imaged by a Fujifilm LAS-4000 imager. Image analysis was performed using Licor Image Studio Lite. Each dot was assigned a value, and the average of two measurements was calculated for each array. The average density values for each cytokine in each condition were then averaged for each array in order to calculate the fold change comparing [−(SC OIS/MLL1 knockdown OIS)], which is shown in blue in Figure 1.

Growth curve measurement

Cells (200,000) were seeded on a 950-mm^2 surface area (one well of a six-well plate) on day 0. Cell number was measured every 2 d with a Countess automated cell counter (Life Technologies) following standard procedures and default parameter settings, after which 200,000 cells were plated back for the next count. Inhibitor or DMSO vehicle control was added on day 0 as cells were seeded and was refreshed every other day as cells were counted and replated. An average of two biological replicates is presented with error bars displaying the standard error of the mean.

RNA-seq

RNA was extracted using RNeasy kit (Qiagen catalog no. 74014) following the manufacturer's instructions. The control (CTL) and OIS libraries were prepared using TruSeq RNA sample preparation kit (catalog no. FC-122-1001) with 1 µg of RNA per sample. The libraries were then sequenced on an Illumina Genome Analyzer IIx platform (36-base-pair [bp] paired-end). Ras control and OIS IMR90s were collected at population doubling 32. The RNA-seq libraries for the SC, SC OIS, and MLL1 knockdown OIS cells were made using a ScriptSeq version 2 RNA-seq library preparation kit from Epicentre (now Illumina) and sequenced using NextSeq platform (50-bp single-end reads) (Illumina). The melanocyte RNA-seq and expression data for uninfected and *BRAF*-infected cells were downloaded from Gene Expression Omnibus (GEO; accession no. GSE46818). All RNA-seq FPKM (fragments per kilobase per million mapped fragments) generation was performed in the following manner: Paired-end data were aligned using RNA STAR version 2.3.0e under default settings, *Homo sapiens* ENSEMBL release 75. Cufflinks version 2.2.1 was used to map reads of the aligned SAM files quantitatively to exons

and gene features (-G parameter). All tRNA, rRNA, and mtRNA transcripts, downloaded from the University of California at Santa Cruz (UCSC) goldenPath database, were masked from the counting procedure. The ENSEMBL *Homo sapiens* release GRCh37.75 was used as the feature table. All other Cufflinks settings were the default parameters. All data were tabulated, averaged, and analyzed using the Python pandas library.

RT-qPCR

RNA was extracted using RNeasy kit (Qiagen) following the manufacturer's instructions. cDNA was obtained and then analyzed by standard qPCR methods on a 7900HT Fast real-time PCR (ABI). Primer sequences are available on request. RT-qPCR data analysis was performed by first obtaining the normalized QT values (normalized to 18S ribosomal RNA). At least three biological replicates were performed for every experiment. For the MLL1 knockdown experiments, the data were transformed across technical and biological replicates to their *z*-scores (mean subtracted, variance divided) to account for the variation in sample material and the reported variability. The Mann-Whitney *U*-test was used to test for and calculate *P*-values for the differences in sample populations between experiments of biological replicates. For all other studies, the average and standard deviations of biological replicates were obtained and assessed for significance using an unpaired *t*-test (http://www.graphpad.com). For all experiments, three asterisks indicates $P < 0.01$, two asterisks indicates $P < 0.05$, one asterisk indicates $P < 0.1$, and NS indicates nonsignificance ($P > 0.1$).

Western blots

Cells were lysed in buffer containing 50 mM Tris (pH 7.5), 0.5 mM EDTA, 150 mM NaCl, 1% NP40, and 2% SDS supplemented with 1:100 Halt protease inhibitor cocktail (Thermo Scientific). The lysates were incubated for 10 min on ice, boiled for 8–10 min at 95°C, and spun down. The supernatant then underwent electrophoresis on a 3%–8% Tris-acetate gel for larger proteins and on a 12% Bis-Tris gel for smaller proteins (NuPAGE). After transfer to nitrocellulose membrane, 5% milk in TBS supplemented with 0.1% Tween 20 (TBST) was used to block the membrane for 1 h at room temperature. Primary antibodies were diluted in 5% BSA in TBST and incubated overnight at 4°C. Primary antibodies are listed below. The membrane was washed three times with TBST for 10 min each followed by incubation of HRP-conjugated secondary antibodies for 1 h at room temperature in 5% BSA/TBST. The membrane was washed again three times and imaged by Fujifilm LAS-4000 imager.

IF

Control and OIS cells were fixed in 4% PFA in PBS for 20 min at room temperature. Cells were washed twice with PBS and permeabilized with 0.5% Triton X-100 in PBS for 10 min. After washing twice, cells were blocked in 10% BSA in PBS for 1 h at room temperature. Cells were incubated with primary antibodies in 5% BSA in PBS supplemented with 0.1% Tween20 (PBST) overnight at 4°C. Antibodies are listed below. Next, cells were washed four times with PBST for 10 min each followed by incubation with fluorophore-conjugated secondary antibody in 5% BSA in PBST for 1 h at room temperature. Cells were then washed three times in PBST and once with PBS and incubated with 1 µg/mL DAPI for 5 min. The cells were then washed twice with PBS and mounted with ProLong Gold (Invitrogen). For the tumor sections, following washes in xylene, ethanol, water, and PBS, sections were treated with target unmasking fluid to deparaffinize

the tissues. Sections were then blocked for 2 h in 3% goat serum followed by incubation in primary antibody overnight. Following secondary antibody incubation and washes, the sections were incubated with 1 µg/mL DAPI for 5 min, washed twice with PBS, and mounted with ProLong Gold with DAPI (Invitrogen). The slides were observed and imaged using a Nikon Eclipse microscope. Microscopy settings were unchanged between SC, SC OIS, and MLL1 knockdown OIS samples as well as between SC and MLL1 shRNA-treated xenograft tumors. For the in vitro cell counts, three independent counts of 100 cells for each condition were performed, and cells were scored positive if they contained at least five positively staining fluorescent nuclear puncta. Similarly, for the tumor sections, three independent 20× fields were scored for positively staining cytokine foci. *P*-values were obtained based on a *t*-test for the relative difference of means (http://www.graphpad.com).

Antibodies

Antibodies included anti-Histone H3 (Abcam, ab1791), anti-Histone H3 (trimethyl K4) (Abcam, ab8580), anti-γH2A.X (phospho-S139) (Abcam, ab2893), anti-IL1α (Abcam, ab9614), anti-IL6 (Developmental Studies Hybridoma Bank, CPTC-IL6-1), anti-phospho-NF-κB p65 (Ser536) (93H1) (Cell Signaling, 3033), anti-ATM (Bethyl Laboratories, A300-299), anti-MLL1 (Bethyl Laboratories, A300-086A), anti-ATM (phospho-S1981) (Abcam, ab81292), anti-β-Tubulin (Sigma, T8328), anti-Ras (Millipore, 05-516), anti-p53 (Pantropic) (Calbiochem, OP43), anti-ATR (Bethyl Laboratories, A300-137A), anti-phospho-p53 (Ser15) (Cell Signaling, 9284), and anti-CDKN2A/p16INK4a (Abcam, ab16123).

Tumor xenograft assay

A total of four male and four female mice (*Mus musculus* strain NOD.Cg-Prkdc[scid] Il2rg[tm1Wjl]/SzJ; Jackson Laboratories, stock no. 005557) between the ages of 38 and 45 d old were used per treatment for tumor xenograft experiments. All animal experiments described adhere to policies and practices approved by the University of Pennsylvania Institutional Biosafety Committee (IBC) and the Institutional Animal Care and Use Committee (IACUC). Cells were collected after shRNA-mediated (MLL1 or SC) knockdowns. Next, 1.5 million cells were injected subcutaneously per mouse. All mice were euthanized 20 wk after subcutaneous injection. Tumors were then excised and frozen. Thirty milligrams of tumor tissue was harvested from each animal for subsequent RNA extraction and RT-qPCR experiments as described above. Tumor sections were cut from formalin-fixed paraffin-embedded tissues and stained for IF as described above. Tumor growth characteristics were as previously reported (Zhu et al. 2015).

Inhibitor assays

The following pharmacologic inhibitors were used: KU55933 (ATM kinase inhibitor) at 10 µM (Selleckchem.com), etoposide at 100 µM (Sigma Aldrich, E1383), and MI-2-2 (MLL1-Menin interaction inhibitor) at 10 and 20 µM (Millipore).

ChIP-seq

Cells in 10-cm² dishes were fixed in 1% formaldehyde for 5 min, and fixation was quenched with addition of glycine to 125 mM for an additional 5 min. Cells were harvested by scraping from plates and were washed twice in 1× PBS before storage at −80°C. ChIP was performed as previously described (Shah et al. 2013) except

that extracts were sonicated nine times for 5 min each round (30 sec of sonication with intermediate incubation of 30 sec per round) using a Bioruptor (Diagenode). All ChIPs were performed using 500 µg of extract and 2 µg of antibody per sample. Thirty microliters of Protein G Dynabeads (Invitrogen, 100.02D) was used per ChIP. ChIP DNA was also used to make sequencing libraries using NEBNext (New England Biolabs). Libraries were quantified (Kapa Biosystems), and sequencing was performed on either Hi-Seq or NextSeq platforms (50-bp, single-end reads) (Illumina). After sequencing, all data were demultiplexed from the raw reads using Illumina's BCL2Fastq version 2.15. Demultiplexed data or Fastq files directly output from a Hi-Seq were aligned to UCSC reference genome build hg19 downloaded from iGenomes. Alignments were generated with Bowtie 2.2.4, allowing for one distinct alignment and one mismatch per seed region (-N1 -K1). All other default parameters were used. Reads were counted to 100-bp fixed bins using featureCounts from the Subreads package version 1.4.6-p2. Normalized TPTM was used. Input was subtracted from γH2A.X, while all H3K4me3 tracks had H3 divided to account for the extensive histone loss seen in senescence. Tracks were visualized using the UCSC genome browser. For Figure 4B, the analysis was done on all genes that had at least a 1.5-fold or greater increase in expression from CTL to OIS as well as at least a 1.5-fold decrease from OIS to MLL1 knockdown OIS cells. Of these genes, the topographic levels of H3K4me3 over the TSS (±1 kb) and γH2A.X over the gene body (normalized by gene length) was counted using the Python package HTSeq version 0.6.1p2. The TSSs of these genes were sorted by mean H3K4me3 fold change enrichment in OIS over CTL cells. The topographic distribution of reads was visualized using Python package Seaborn version 0.5.1. The heat maps show $\log_2$ fold change of (in order from left to right) H3K4me3 in OIS over CTL cells, H3K4me3 in MLL1 knockdown OIS over OIS cells, γH2A.X in OIS over CTL cells, and γH2A.X in MLL1 knockdown OIS over OIS cells. The final heat map is the visualization of the RNA-seq $\log_2$ fold change in OIS over CTL and MLL1 knockdown OIS over OIS. For Supplemental Figure S3A, aligned ChIP-seq reads were mapped to features using the ENSEMBL GRCh37.75 gene table (GTF from iGenomes). The top 1% of the most highly up-regulated genes in OIS was then calculated, identified by taking the log of the fold change of OIS expression over control expression. The log of the fold change in OIS over control of the γH2A.X and H3K4me3 read density over these genes was then calculated. The joint relationship between the expression and the γH2AX fold change was plotted. The genes were then colored by their relative fold change in H3K4me3.

TCGA analysis

RNA-seq data sets from breast invasive carcinoma and prostate adenocarcinoma were obtained from TCGA (https://tcga-data.nci.nih.gov/tcga). Original RNA expression values (normalized read counts) were used for downstream analyses. For each cancer type, samples were ranked by MLL1 expression levels and were evenly divided into three groups. Comparisons were performed between the group of samples with the highest MLL1 expression and the group of samples with lowest MLL1 expression. One-sided Wilcoxon rank sum tests were used to compute significance. For the ATM analyses, TCGA data were derived from cBioPortal for Cancer Genomics (http://www.cbioportal.org) (Cerami et al. 2012; Gao et al. 2013), and scatter plots were generated by querying all cancers that have RNA-seq expression data and generating lists of genes coexpressed with *ATM*. We ranked the cancers by their specific Pearson correlation between *ATM* and *MLL1* and then ranked the mean Pearson correlation among all of the cancers for each gene and placed the genes in rank order.

References

Acosta JC, Banito A, Wuestefeld T, Georgilis A, Janich P, Morton JP, Athineos D, Kang TW, Lasitschka F, Andrulis M, et al. 2013. A complex secretory program orchestrated by the inflammasome controls paracrine senescence. *Nat Cell Biol* **15:** 978–990.

Agger K, Cloos PA, Rudkjaer L, Williams K, Andersen G, Christensen J, Helin K. 2009. The H3K27me3 demethylase JMJD3 contributes to the activation of the INK4A–ARF locus in response to oncogene- and stress-induced senescence. *Genes Dev* **23:** 1171–1176.

Algire C, Moiseeva O, Deschenes-Simard X, Amrein L, Petruccelli L, Birman E, Viollet B, Ferbeyre G, Pollak MN. 2012. Metformin reduces endogenous reactive oxygen species and associated DNA damage. *Cancer Prev Res* **5:** 536–543.

Barradas M, Anderton E, Acosta JC, Li S, Banito A, Rodriguez-Niedenfuhr M, Maertens G, Banck M, Zhou MM, Walsh MJ, et al. 2009. Histone demethylase JMJD3 contributes to epigenetic control of INK4a/ARF by oncogenic RAS. *Genes Dev* **23:** 1177–1182.

Blobel GA, Kadauke S, Wang E, Lau AW, Zuber J, Chou MM, Vakoc CR. 2009. A reconfigured pattern of MLL occupancy within mitotic chromatin promotes rapid transcriptional reactivation following mitotic exit. *Mol Cell* **36:** 970–983.

Borkin D, He S, Miao H, Kempinska K, Pollock J, Chase J, Purohit T, Malik B, Zhao T, Wang J, et al. 2015. Pharmacologic inhibition of the Menin–MLL interaction blocks progression of MLL leukemia in vivo. *Cancer Cell* **27:** 589–602.

Bracken AP, Kleine-Kohlbrecher D, Dietrich N, Pasini D, Gargiulo G, Beekman C, Theilgaard-Monch K, Minucci S, Porse BT, Marine JC, et al. 2007. The Polycomb group proteins bind throughout the INK4A–ARF locus and are disassociated in senescent cells. *Genes Dev* **21:** 525–530.

Cahu J, Bustany S, Sola B. 2012. Senescence-associated secretory phenotype favors the emergence of cancer stem-like cells. *Cell Death Dis* **3:** e446.

Canino C, Mori F, Cambria A, Diamantini A, Germoni S, Alessandrini G, Borsellino G, Galati R, Battistini L, Blandino R, et al. 2012. SASP mediates chemoresistance and tumor-initiating-activity of mesothelioma cells. *Oncogene* **31:** 3148–3163.

Cerami E, Gao J, Dogrusoz U, Gross BE, Sumer SO, Aksoy BA, Jacobsen A, Byrne CJ, Heuer ML, Larsson E, et al. 2012. The cBio cancer genomics portal: an open platform for exploring multidimensional cancer genomics data. *Cancer Discov* **2:** 401–404.

Cerqueira A, Santamaria D, Martinez-Pastor B, Cuadrado M, Fernandez-Capetillo O, Barbacid M. 2009. Overall Cdk activity modulates the DNA damage response in mammalian cells. *J Cell Biol* **187:** 773–780.

Chien Y, Scuoppo C, Wang X, Fang X, Balgley B, Bolden JE, Premsrirut P, Luo W, Chicas A, Lee CS, et al. 2011. Control of the senescence-associated secretory phenotype by NF-κB promotes senescence and enhances chemosensitivity. *Genes Dev* **25:** 2125–2136.

Coppe JP, Kauser K, Campisi J, Beausejour CM. 2006. Secretion of vascular endothelial growth factor by primary human fibroblasts at senescence. *J Biol Chem* **281:** 29568–29574.

Coppe JP, Desprez PY, Krtolica A, Campisi J. 2010. The senescence-associated secretory phenotype: the dark side of tumor suppression. *Annu Rev Pathol* **5:** 99–118.

Coppe JP, Rodier F, Patil CK, Freund A, Desprez PY, Campisi J. 2011. Tumor suppressor and aging biomarker p16(INK4a) induces cellular senescence without the associated inflammatory secretory phenotype. *J Biol Chem* **286:** 36396–36403.

Crusz SM, Balkwill FR. 2015. Inflammation and cancer: advances and new agents. *Nat Rev Clin Oncol* **12:** 584–596.

d'Adda di Fagagna F. 2008. Living on a break: cellular senescence as a DNA-damage response. *Nat Rev Cancer* **8:** 512–522.

Dankort D, Filenova E, Collado M, Serrano M, Jones K, McMahon M. 2007. A new mouse model to explore the initiation, progression, and therapy of BRAFV600E-induced lung tumors. *Genes Dev* **21:** 379–384.

Di Micco R, Fumagalli M, Cicalese A, Piccinin S, Gasparini P, Luise C, Schurra C, Garre M, Nuciforo PG, Bensimon A, et al. 2006. Oncogene-induced senescence is a DNA damage response triggered by DNA hyper-replication. *Nature* **444:** 638–642.

Freund A, Orjalo AV, Desprez PY, Campisi J. 2010. Inflammatory networks during cellular senescence: causes and consequences. *Trends Mol Med* **16:** 238–246.

Freund A, Patil CK, Campisi J. 2011. p38MAPK is a novel DNA damage response-independent regulator of the senescence-associated secretory phenotype. *EMBO J* **30:** 1536–1548.

Gao J, Aksoy BA, Dogrusoz U, Dresdner G, Gross B, Sumer SO, Sun Y, Jacobsen A, Sinha R, Larsson E, et al. 2013. Integrative analysis of complex cancer genomics and clinical profiles using the cBioPortal. *Sci Signal* **6:** pl1.

Gentles AJ, Newman AM, Liu CL, Bratman SV, Feng W, Kim D, Nair VS, Xu Y, Khuong A, Hoang CD, et al. 2015. The prognostic landscape of genes and infiltrating immune cells across human cancers. *Nat Med* **21:** 938–945.

Gorgoulis VG, Vassiliou LV, Karakaidos P, Zacharatos P, Kotsinas A, Liloglou T, Venere M, Ditullio RA Jr, Kastrinakis NG, Levy B, et al. 2005. Activation of the DNA damage checkpoint and genomic instability in human precancerous lesions. *Nature* **434:** 907–913.

Hanahan D, Weinberg RA. 2011. Hallmarks of cancer: the next generation. *Cell* **144:** 646–674.

Huang TT, Wuerzberger-Davis SM, Wu ZH, Miyamoto S. 2003. Sequential modification of NEMO/IKKγ by SUMO-1 and ubiquitin mediates NF-κB activation by genotoxic stress. *Cell* **115:** 565–576.

Huang J, Gurung B, Wan B, Matkar S, Veniaminova NA, Wan K, Merchant JL, Hua X, Lei M. 2012. The same pocket in menin binds both MLL and JUND but has opposite effects on transcription. *Nature* **482:** 542–546.

Imai T, Yamauchi M, Seki N, Sugawara T, Saito T, Matsuda Y, Ito H, Nagase T, Nomura N, Hori T. 1996. Identification and characterization of a new gene physically linked to the ATM gene. *Genome Res* **6:** 439–447.

Jenei V, Sherwood V, Howlin J, Linnskog R, Safholm A, Axelsson L, Andersson T. 2009. A t-butyloxycarbonyl-modified Wnt5a-derived hexapeptide functions as a potent antagonist of Wnt5a-dependent melanoma cell invasion. *Proc Natl Acad Sci* **106:** 19473–19478.

Johnson N, Shapiro GI. 2010. Cyclin-dependent kinases (cdks) and the DNA damage response: rationale for cdk inhibitor-chemotherapy combinations as an anticancer strategy for solid tumors. *Expert Opin Therap Targets* **14:** 1199–1212.

Justus CR, Leffler N, Ruiz-Echevarria M, Yang LV. 2014. In vitro cell migration and invasion assays. *J Vis Exp* doi: 10.3791/51046.

Katada S, Sassone-Corsi P. 2010. The histone methyltransferase MLL1 permits the oscillation of circadian gene expression. *Nat Struct Mol Biol* **17:** 1414–1421.

Kuilman T, Michaloglou C, Vredeveld LC, Douma S, van Doorn R, Desmet CJ, Aarden LA, Mooi WJ, Peeper DS. 2008. Oncogene-induced senescence relayed by an interleukin-dependent inflammatory network. *Cell* **133:** 1019–1031.

Laberge RM, Awad P, Campisi J, Desprez PY. 2012. Epithelial–mesenchymal transition induced by senescent fibroblasts. *Cancer Microenviron* **5:** 39–44.

Liu H, Takeda S, Kumar R, Westergard TD, Brown EJ, Pandita TK, Cheng EH, Hsieh JJ. 2010. Phosphorylation of MLL by ATR is required for execution of mammalian S-phase checkpoint. *Nature* **467:** 343–346.

Madabhushi R, Gao F, Pfenning AR, Pan L, Yamakawa S, Seo J, Rueda R, Phan TX, Yamakawa H, Pao PC, et al. 2015. Activity-induced DNA breaks govern the expression of neuronal early-response genes. *Cell* **161:** 1592–1605.

Malik R, Khan AP, Asangani IA, Cieslik M, Prensner JR, Wang X, Iyer MK, Jiang X, Borkin D, Escara-Wilke J, et al. 2015. Targeting the MLL complex in castration-resistant prostate cancer. *Nat Med* **21:** 344–352.

Michaloglou C, Vredeveld LC, Soengas MS, Denoyelle C, Kuilman T, van der Horst CM, Majoor DM, Shay JW, Mooi WJ, Peeper DS. 2005. BRAFE600-associated senescence-like cell cycle arrest of human naevi. *Nature* **436:** 720–724.

Milne TA, Briggs SD, Brock HW, Martin ME, Gibbs D, Allis CD, Hess JL. 2002. MLL targets SET domain methyltransferase activity to Hox gene promoters. *Mol Cell* **10:** 1107–1117.

Moiseeva O, Deschenes-Simard X, St-Germain E, Igelmann S, Huot G, Cadar AE, Bourdeau V, Pollak MN, Ferbeyre G. 2013. Metformin inhibits the senescence-associated secretory phenotype by interfering with IKK/NF-κB activation. *Aging Cell* **12:** 489–498.

Munoz-Espin D, Serrano M. 2014. Cellular senescence: from physiology to pathology. *Nat Rev Mol Cell Biol* **15:** 482–496.

Neves J, Demaria M, Campisi J, Jasper H. 2015. Of flies, mice, and men: evolutionarily conserved tissue damage responses and aging. *Dev Cell* **32:** 9–18.

Obenauf AC, Zou Y, Ji AL, Vanharanta S, Shu W, Shi H, Kong X, Bosenberg MC, Wiesner T, Rosen N, et al. 2015. Therapy-induced tumour secretomes promote resistance and tumour progression. *Nature* **520:** 368–372.

Orjalo AV, Bhaumik D, Gengler BK, Scott GK, Campisi J. 2009. Cell surface-bound IL-1α is an upstream regulator of the senescence-associated IL-6/IL-8 cytokine network. *Proc Natl Acad Sci* **106:** 17031–17036.

Piret B, Schoonbroodt S, Piette J. 1999. The ATM protein is required for sustained activation of NF-κB following DNA damage. *Oncogene* **18:** 2261–2271.

Rao RC, Dou Y. 2015. Hijacked in cancer: the KMT2 (MLL) family of methyltransferases. *Nat Rev Cancer* **15:** 334–346.

Rodier F, Campisi J. 2011. Four faces of cellular senescence. *J Cell Biol* **192:** 547–556.

Rodier F, Coppe JP, Patil CK, Hoeijmakers WA, Munoz DP, Raza SR, Freund A, Campeau E, Davalos AR, Campisi J. 2009. Persistent DNA damage signalling triggers senescence-associated inflammatory cytokine secretion. *Nat Cell Biol* **11:** 973–979.

Rogakou EP, Boon C, Redon C, Bonner WM. 1999. Megabase chromatin domains involved in DNA double-strand breaks in vivo. *J Cell Biol* **146:** 905–916.

Serrano M, Lin AW, McCurrach ME, Beach D, Lowe SW. 1997. Oncogenic ras provokes premature cell senescence associated with accumulation of p53 and p16INK4a. *Cell* **88:** 593–602.

Shah PP, Donahue G, Otte GL, Capell BC, Nelson DM, Cao K, Aggarwala V, Cruickshanks HA, Rai TS, McBryan T, et al. 2013. Lamin B1 depletion in senescent cells triggers large-scale changes in gene expression and the chromatin landscape. *Genes Dev* **27:** 1787–1799.

Shalapour S, Karin M. 2015. Immunity, inflammation, and cancer: an eternal fight between good and evil. *J Clin Invest* **125:** 3347–3355.

Sheu JJ, Guan B, Tsai FJ, Hsiao EY, Chen CM, Seruca R, Wang TL, Shih Ie M. 2012. Mutant BRAF induces DNA strand breaks, activates DNA damage response pathway, and up-regulates glucose transporter-1 in nontransformed epithelial cells. *Am J Pathol* **180:** 1179–1188.

Shintomi K, Takahashi TS, Hirano T. 2015. Reconstitution of mitotic chromatids with a minimum set of purified factors. *Nat Cell Biol* **17:** 1014–1023.

Sivakumar S, Gorbsky GJ. 2015. Spatiotemporal regulation of the anaphase-promoting complex in mitosis. *Nat Rev Mol Cell Biol* **16:** 82–94.

Sun Y, Campisi J, Higano C, Beer TM, Porter P, Coleman I, True L, Nelson PS. 2012. Treatment-induced damage to the tumor microenvironment promotes prostate cancer therapy resistance through WNT16B. *Nat Med* **18:** 1359–1368.

Takeda S, Chen DY, Westergard TD, Fisher JK, Rubens JA, Sasagawa S, Kan JT, Korsmeyer SJ, Cheng EH, Hsieh JJ. 2006. Proteolysis of MLL family proteins is essential for taspase1-orchestrated cell cycle progression. *Genes Dev* **20:** 2397–2409.

Tian B, Yang Q, Mao Z. 2009. Phosphorylation of ATM by Cdk5 mediates DNA damage signalling and regulates neuronal death. *Nat Cell Biol* **11:** 211–218.

van Deursen JM. 2014. The role of senescent cells in ageing. *Nature* **509:** 439–446.

Walter MN, Wright KT, Fuller HR, MacNeil S, Johnson WE. 2010. Mesenchymal stem cell-conditioned medium accelerates skin wound healing: an in vitro study of fibroblast and keratinocyte scratch assays. *Exp Cell Res* **316:** 1271–1281.

Wang B, Hendricks DT, Wamunyokoli F, Parker MI. 2006. A growth-related oncogene/CXC chemokine receptor 2 autocrine loop contributes to cellular proliferation in esophageal cancer. *Cancer Res* **66:** 3071–3077.

Wang P, Han L, Shen H, Wang P, Lv C, Zhao G, Niu J, Xue L, Wang QJ, Tong T, et al. 2014. Protein kinase D1 is essential for Ras-induced senescence and tumor suppression by regulating senescence-associated inflammation. *Proc Natl Acad Sci* **111:** 7683–7688.

Wu ZH, Shi Y, Tibbetts RS, Miyamoto S. 2006. Molecular linkage between the kinase ATM and NF-κB signaling in response to genotoxic stimuli. *Science* **311:** 1141–1146.

Yew TL, Hung YT, Li HY, Chen HW, Chen LL, Tsai KS, Chiou SH, Chao KC, Huang TF, Chen HL, et al. 2011. Enhancement of wound healing by human multipotent stromal cell conditioned medium: the paracrine factors and p38 MAPK activation. *Cell Transplant* **20:** 693–706.

Zelenay S, van der Veen AG, Bottcher JP, Snelgrove KJ, Rogers N, Acton SE, Chakravarty P, Girotti MR, Marais R, Quezada SA, et al. 2015. Cyclooxygenase-dependent tumor growth through evasion of immunity. *Cell* **162:** 1257–1270.

Zhu J, Woods D, McMahon M, Bishop JM. 1998. Senescence of human fibroblasts induced by oncogenic Raf. *Genes Dev* **12:** 2997–3007.

Zhu J, Sammons MA, Donahue G, Dou Z, Vedadi M, Getlik M, Barsyte-Lovejoy D, Al-awar R, Katona BW, Shilatifard A, et al. 2015. Gain-of-function p53 mutants co-opt chromatin pathways to drive cancer growth. *Nature* **525:** 206–211.

MLL1 is essential for the senescence-associated secretory phenotype

Brian C. Capell, Adam M. Drake, Jiajun Zhu, et al.

Supplemental Material	http://genesdev.cshlp.org/content/suppl/2016/01/29/30.3.321.DC1
References	This article cites 67 articles, 23 of which can be accessed free at: http://genesdev.cshlp.org/content/30/3/321.full.html#ref-list-1
Creative Commons License	This article is distributed exclusively by Cold Spring Harbor Laboratory Press for the first six months after the full-issue publication date (see http://genesdev.cshlp.org/site/misc/terms.xhtml). After six months, it is available under a Creative Commons License (Attribution-NonCommercial 4.0 International), as described at http://creativecommons.org/licenses/by-nc/4.0/.
Email Alerting Service	Receive free email alerts when new articles cite this article - sign up in the box at the top right corner of the article or **click here.**